Extracting the Response of the Bay Bridge, California, from the Application of Multichannel Deconvolution to Earthquake-Induced Shaking

Jing Jian[1], Roel Snieder[*1], and Nori Nakata[2]

ABSTRACT

Engineered structures, such as bridges, are excited by earthquakes at the base of the towers and the endpoint of decks. The different structural units of bridges, such as the towers and decks, are coupled. We extract the response of the towers and decks of the Bay Bridge in California from the motion of the bridge that is caused by earthquakes. This constitutes a multichannel deconvolution problem, which is, in general, ill-posed. We use the redundancy of the western half of the Bay Bridge, with near-identical towers and decks, to estimate the response of the upper towers, lower towers, and decks, from the transverse motion recorded in the bridge after four earthquakes. The extracted response functions for the four earthquakes show consistent wave arrivals that correspond to the waves that propagate through the towers and the decks. This method can, in principle, be used to monitor changes in the structural response.

KEY POINTS

- We examine the structural response of the Bay Bridge, San Francisco, from earthquake recordings.
- We extract the response of the towers and decks using multichannel deconvolution.
- The method can, in principle, be used for structural monitoring over time.

INTRODUCTION

Earthquakes and ambient noise have been used to extract the mechanical properties of bridges and buildings. Early studies of buildings used resonant frequencies (Carder, 1936). One of the early studies of the vibrations in bridges was applied to the Bay Bridge (Carder, 1937), which is also the object of this study. Many studies of bridges and buildings (e.g., Udwadia and Trifunac, 1974; Luco *et al.*, 1987; Kohler *et al.*, 2005; Clinton *et al.*, 2006; Lynch *et al.*, 2006) focused on the resonances and changes in the resonant frequencies. An overview of testing and monitoring of buildings and bridges is given in recent books (Wenzel, 2009; Conte *et al.*, 2018). The resonant frequency is a property of the whole structure, but it does not necessarily provide information about subunits such as the towers or decks of a bridge.

Extracting the response of systems from ambient vibrations took a leap forward with the development of seismic interferometry (Curtis *et al.*, 2006; Larose *et al.*, 2006; Snieder and Larose, 2013) in which the cross correlation of ambient noise recorded at two locations gives the Green's function that characterizes the response between these locations. Because ambient noise is present most of the time, this technique is particularly useful for monitoring time-lapse changes. An application to bridge monitoring is shown by Salvermoser *et al.* (2015).

In addition to cross correlation, deconvolution of the recorded motion in structures has been used to extract the response of buildings. This was applied to the recordings of earthquakes (Snieder and Şafak, 2006; Kohler *et al.*, 2007; Nakata *et al.*, 2013) and to measurements of ambient noise (Prieto *et al.*, 2010; Nakata and Snieder, 2014). One of the advantages of this technique is that it makes it possible to retrieve the structural response under boundary conditions different from those of the real structure (Snieder *et al.*, 2006). Recent studies relate the resonances of buildings to the response obtained from deconvolution (Bindi *et al.*, 2015; Sun *et al.*, 2017). Recordings of ambient noise, or of subsequent earthquakes, have been used to detect time-lapse changes in buildings or bridges (Trifunac *et al.*, 2003; Nakata *et al.*, 2015; Salvermoser *et al.*, 2015) that are essentially 1D on the scale of the used wavelength. Our work extends the extraction of the response of a building by deconvolution

1. Center for Wave Phenomena, Colorado School of Mines, Golden, Colorado, U.S.A.; 2. Massachusetts Institute of Technology, Cambridge, Massachusetts, U.S.A.

*Corresponding author: rsnieder@mines.edu

Cite this article as Jian, J., R. Snieder, and N. Nakata (2020). Extracting the Response of the Bay Bridge, California, from the Application of Multichannel Deconvolution to Earthquake-Induced Shaking, *Bull. Seismol. Soc. Am.* **XX**, 1–9, doi: 10.1785/0120190231

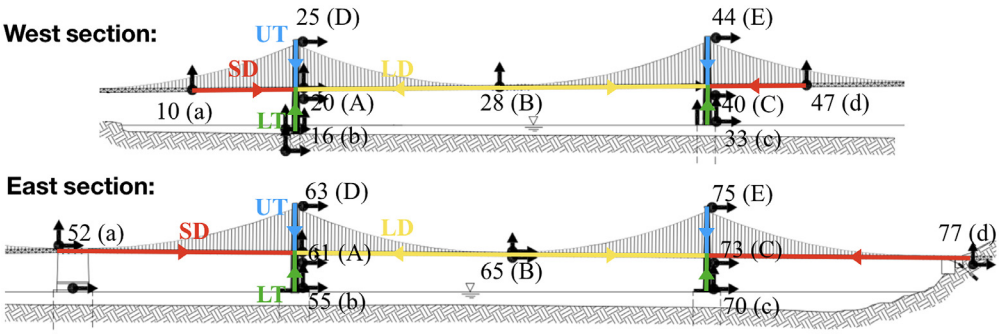

Figure 1. Geometry of the west and east sections of the western half of the Bay Bridge with the location of the used accelerometers, and the structural units the transfer function of which we solve for. LT, lower towers; SD, short decks; UT, upper towers. The color version of this figure is available only in the electronic edition.

(Snieder and Şafak, 2006) to the Bay Bridge, which cannot be treated as a 1D structure.

We use multichannel deconvolution to extract the structural response of the towers and decks of the western half of the Bay Bridge in California. The western half of the Bay Bridge extends from San Francisco to Yerba Buena Island, whereas the eastern half of the bridge connects Yerba Buena Island to Oakland. The western half of the Bay Bridge consists of two suspension bridges with two towers each that are separated by a rock pillar. In the following, we analyze the response of the western half of the Bay Bridge. The western half consists of two parts, each with two towers, and we refer to these two parts as the west section and the east section (Fig. 1).

In deconvolution studies applied to structures, one deconvolves the recorded motion at two locations to retrieve the transfer function of the structure between those locations (Snieder and Şafak, 2006). In this approach the deconvolution has one input and one output, which gives one transfer function. For tall buildings, where the wave propagation at low frequencies is approximately 1D, this approach is applicable because the waves propagate only upward and downward between these points. In a bridge with different structural elements, however, the motion at one point depends on waves coming in from different directions. For example, the motion in the middle of the bridge deck depends on waves being launched at pillars on both sides of the deck. The motion in the pillars, in turn, depends on the waves coming in from the subsurface, from the decks on both sides of the pillar, and possible from the towers above the bridge deck. In this case there is not a single transfer function, but a transfer matrix that relates the response in the different structural units of the bridge.

The estimation of the transfer matrix corresponds to multichannel deconvolution. Suppose one has N_{in} input channels and N_{out} output channels, then one has $N_{\text{in}} + N_{\text{out}}$ pieces of information. The transfer function has $N_{\text{in}} \times N_{\text{out}}$ unknowns. For normal deconvolution $N_{\text{in}} = N_{\text{out}} = 1$, and there is one transfer function. But when there are more channels the number of unknowns exceeds the number of data points, and multichannel deconvolution is ill-posed. This ill-posedness can be countered by regularization (e.g., Kirkeby *et al.*, 1998; Du *et al.*, 2018). We circumvent the ill-posedness of the estimation of the structural response of the Bay Bridge by assuming that comparable structural elements of the Bay Bridge are similar. For example, we assume that the two towers on the western part of the bridge have an identical response, and that the two halves of the long decks (LDs) between the towers and the midpoint of the decks also have the same response. We show that this assumption leads to a system of five linear equations with four unknowns; thus, the system is overdetermined rather than underdetermined. We solve this system in the least-squares sense and apply Tikhonov regularization to prevent instabilities in the extracted bridge response.

In this study, we use the motion of the bridge excited by earthquakes to extract the response of the bridge. Internal noise, such as wind noise or traffic on the deck, complicates the analysis. For example, noise generated by vehicles on the deck at the midpoint between two sensors arrives simultaneously at these two sensors and will, therefore, give a contribution at zero lag time to the extracted response. Because the wave velocity is finite, this does not correspond to a wave that propagates between these sensors. For this reason, we limit the analysis to earthquake-induced motion that is excited externally at the points of contact of the bridge with the subsurface. Nakata and Snieder (2014) show how to use internal noise for the extraction of the response of a building.

We first present the used earthquake data and then show how a system of linear equations can be used to extract the transfer function of the Bay Bridge from recorded vibrations. We then show the extracted transfer functions of the upper towers (UTs), lower towers (LTs), and different decks.

USED DATA

The motion of the Bay Bridge is measured with 77 accelerometers, and we used the motion in the bridge caused by the earthquakes shown in Table 1. The data were made available by the Center for Engineering Strong Motion Data. In this study, we only analyze the recorded motion in the transverse direction, the horizontal motion perpendicular to the direction of the bridge. Thus, the extracted transfer functions are for the transverse motion of the bridge. The reason for this restriction is that we ignore the influence of the cables in our analysis. As shown in Figure 2, a vertical motion of the deck is transmitted

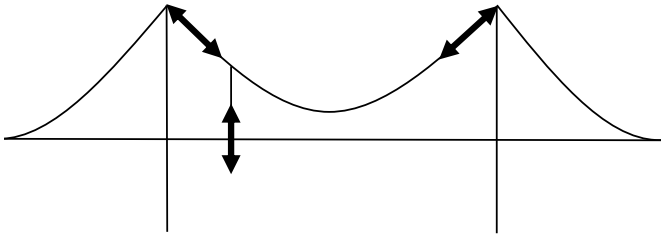

Figure 2. Schematic that illustrates how the vertical motion of the deck is coupled by the support cables to the vertical and horizontal inline motion at the top of the towers. The figure is not to scale, and for simplicity we show only one vertical cable.

by the cables to a motion of the top of the towers that has both a horizontal and vertical component in the vertical plane through the bridge. The theory presented here does not account for the coupling of the motion at different locations of the bridge by the cables. In addition, at the intersection of the towers and the decks, the vertical motion and the inline horizontal motion is coupled, which also necessitates modifications to the theory we present. These complications are avoided when using the motion in the transverse direction, for which the coupling to the motion in vertical direction and inline horizontal direction can be ignored.

Examples of the transverse motion after the Alum Rock earthquake are shown in Figure 3. To eliminate high-frequency noise in the data, we applied a low-pass Butterworth filter at 40 Hz. A Tukey window is applied to taper the first and last 10% of each recording, and zeros were padded at the end of each recording to obtain a uniform record length of 116 s. The motion recorded for the South Napa earthquake was sampled at a lower sampling rate than the other earthquakes (Table 1) and was interpolated so that all time series had a uniform sampling rate of 200 Hz. As shown in Figure 3, the used waveforms are complicated and consist of a combination of *P* waves, *S* waves, and surface waves, which have been scattered and mode-converted. Apart from low-pass filtering, we simply use the full waveforms in the analysis, because it does not matter which wave type excites the bridge; only the net motion at the points of contact of the bridge with the subsurface is important.

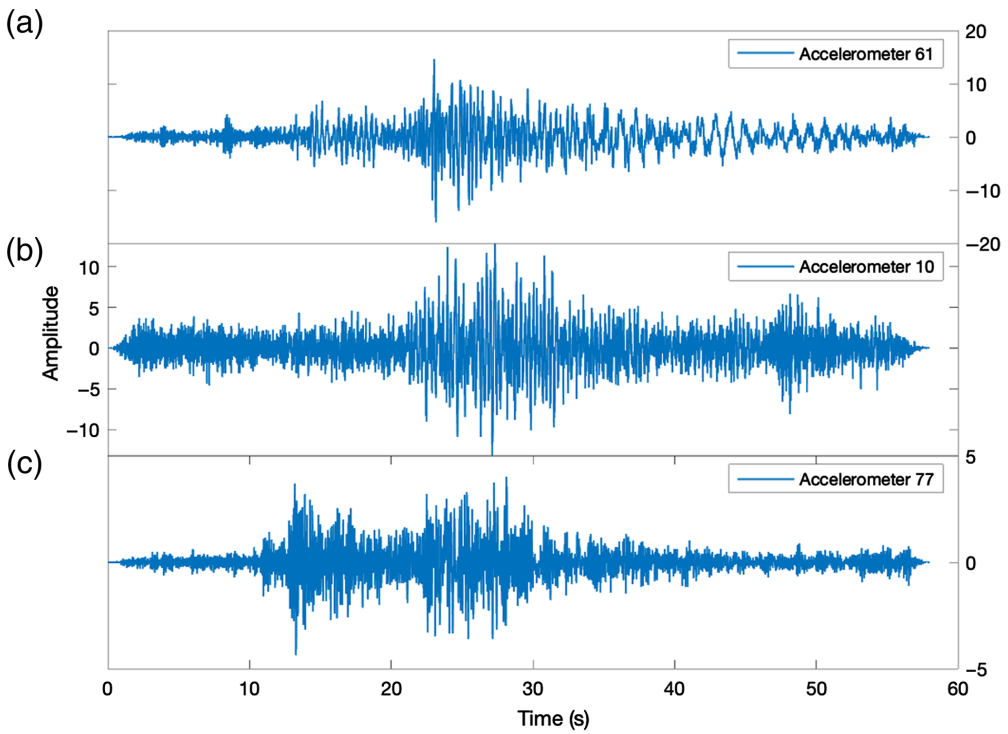

Figure 3. Transverse motion at three accelerometers (in centimeters per second) caused by the Alum Rock earthquake recorded at the intersection of (a) the deck and the west tower of the east section, (b) the small deck on the west of the west section, and (c) the connection of the east section with the shore. The color version of this figure is available only in the electronic edition.

TABLE 1
Earthquakes Used with Origin Time, Epicentral Distance, Magnitude, the Data Length, and Sampling Rate of the Used Time Series

Earthquake	Time (yyyy/mm/dd hh:mm:ss)	Distance (km)	Magnitude	Data Length (s)	Sampling Rate (Hz)
Alum Rock	2007/10/31 03:04:54	67.74	5.6	58	200
Berkeley	2011/10/20 21:41:04	12.04	4.0	56	200
Piedmont	2015/08/17 13:49:17	11.05	4.0	56	200
South Napa	2014/08/24 10:20:44	46.32	6.0	78	100

TABLE 2
Structural Units of the West Section the Transfer Function of which We Estimate

Structural Unit	Name	Segment	Length (m)	Velocity (m/s)
Short deck	SD	aA, dC	178.5, 176.8	n/a
Long deck	LD	AB, CB	352.1, 352.1	651
Lower tower	LT	bA, cC	43.0, 46.5	895
Upper tower	UT	AD, CE	83.0, 93.0	510

The structural units refer to Figure 1.

EXTRACTING THE RESPONSE OF STRUCTURAL UNITS

In contrast to a tall building, which essentially is a 1D structure, a bridge consists of a number of structural elements, and the motion of these structural elements is, in general, coupled. Instead of a transfer function, one thus has to solve for a transfer matrix, and as shown in the Introduction, this leads, in general, to an ill-posed linear system of equations. We avoid this ill-posedness by assuming that the mechanical response of the different towers and decks is identical. We describe below the retrieval of the response of the west section of the bridge (upper panel in Fig. 1), but we apply the same analysis to the east section of the bridge (lower panel in Fig. 1). A comparison of the response of the structural units in the west section and the east section provides a consistency check of the used analysis.

In the following, we retrieve the response of the UTs, the LTs, the LDs, and the short decks (SDs), in which the different structural units are shown in Figure 1. For the west section, the properties of these units are summarized in Table 2. In reality, the corresponding structural units at different locations, such as the different UTs, differ in length by less than 10%. Because of the finite bandwidth of the used data, the retrieved time-domain response of the units shows peaks the width of which is more than 10% of the arrival time of these peaks. The error in the travel time caused by the differences in the length of the structural units can thus not be resolved anyhow with the bandwidth of the used data.

In the following, we denote the response of the UTs by G_{UT} and use a similar notation for the LTs, the SD, and the LD. The derivation below is in the frequency domain and applies to the west section of the bridge, but the same reasoning applies to the east section. Consider, for example, the motion in sensor 20 at the intersection of the westmost tower and the deck (Fig. 1). The motion at sensor 20 is influenced by waves propagating to the right from the SD, by waves propagating to the left in the LD, by waves propagating downward from the UT, and propagating upward in the LT. Consider, as an example, the waves propagating rightward from the SD. The contribution of these waves to the motion $u_{20}(\omega)$ at the intersection of the westmost tower and the deck is given by the motion $u_{10}(\omega)$ recorded in the SD times the response $G_{\mathrm{SD}}(\omega)$ of the SD, giving a total contribution $G_{\mathrm{SD}}(\omega)u_{10}(\omega)$ to the motion $u_{20}(\omega)$. Adding the contributions of the four waves that move toward sensor 20 gives the top equation of the following system:

$$
\begin{aligned}
u_{20}(\omega) &= G_{\mathrm{SD}}(\omega)u_{10}(\omega) + G_{\mathrm{LT}}(\omega)u_{16}(\omega) + G_{\mathrm{LD}}(\omega)u_{28}(\omega) \\
&\quad + G_{\mathrm{UT}}(\omega)u_{25}(\omega), \\
u_{25}(\omega) &= \frac{1}{G_{\mathrm{UT}}(\omega)}u_{20}(\omega), \\
u_{28}(\omega) &= \frac{1}{G_{\mathrm{LD}}(\omega)}u_{20}(\omega) + \frac{1}{G_{\mathrm{LD}}(\omega)}u_{40}(\omega), \\
u_{40}(\omega) &= G_{\mathrm{SD}}(\omega)u_{47}(\omega) + G_{\mathrm{LT}}(\omega)u_{33}(\omega) + G_{\mathrm{LD}}(\omega)u_{28}(\omega) \\
&\quad + G_{\mathrm{UT}}(\omega)u_{44}(\omega), \\
u_{44}(\omega) &= \frac{1}{G_{\mathrm{UT}}(\omega)}u_{40}(\omega). \qquad (1)
\end{aligned}
$$

The transfer function between the motion at points A and B is defined as $G_{AB}(\omega) = u_A(\omega)/u_B(\omega)$. It follows from this definition that

$$
G_{AB}(\omega) = 1/G_{BA}(\omega). \qquad (2)
$$

The response of the UT is, in the frequency domain, defined as the ratio of the motion at base of the UT to the motion at the top of the UT. For the western tower of the west section this gives with the property (2) the second equation in the system (1). The response G_{LD} of the long deck is defined as the ratio of the motion at the point of intersection of the tower-end of the deck to the motion in the middle of the deck. With property (2), this implies that $1/G_{\mathrm{LD}}$ is the ratio of the motion in the middle of the deck to the motion at the endpoint of the deck. Referring to Figure 1, this gives for the western long deck the third equation of the system (1), in which we used that the motion in the middle of the long deck is influenced by the waves coming in from both towers. The last two equations of the system (1) follow by applying the same reasoning to the eastern half of the west section of bridge.

The linear system (1) can be rewritten as

$$
\mathbf{y} = \mathbf{A}\mathbf{x}, \qquad (3)
$$

with

$$
\mathbf{y} = \begin{pmatrix} u_{20}(\omega) \\ u_{20}(\omega) \\ u_{20}(\omega) + u_{40}(\omega) \\ u_{40}(\omega) \\ u_{40}(\omega) \end{pmatrix}, \qquad \mathbf{x} = \begin{pmatrix} G_{\mathrm{SD}}(\omega) \\ G_{\mathrm{LT}}(\omega) \\ G_{\mathrm{LD}}(\omega) \\ G_{\mathrm{UT}}(\omega) \end{pmatrix} \qquad (4)
$$

and

$$
\mathbf{A} = \begin{pmatrix} u_{10}(\omega) & u_{16}(\omega) & u_{28}(\omega) & u_{25}(\omega) \\ 0 & 0 & 0 & u_{25}(\omega) \\ 0 & 0 & u_{28}(\omega) & 0 \\ u_{47}(\omega) & u_{33}(\omega) & u_{28}(\omega) & u_{44}(\omega) \\ 0 & 0 & 0 & u_{44}(\omega) \end{pmatrix}. \qquad (5)
$$

Equation (3) constitutes a linear system of equations in which $\mathbf{y}$ and the matrix $\mathbf{A}$ are determined by the data, and that contains the transfer functions in the vector $\mathbf{x}$. This system is overdetermined; thus, we compute the damped least-squares solution

$$\mathbf{x}_{LS} = (\mathbf{A}^{\dagger}\mathbf{A} + \varepsilon\mathbf{I})^{-1}\mathbf{A}^{\dagger}\mathbf{y}, \quad (6)$$

in which the dagger denotes the Hermitian adjoint and $\mathbf{I}$ is the identity matrix. The regularization parameter is chosen to be $\varepsilon = \gamma\lambda_{\max}$, in which $\lambda_{\max}$ is the largest eigenvalue of $\mathbf{A}^{\dagger}\mathbf{A}$ for all the frequencies considered. In the examples shown here we used $\gamma = 5\%$ because we found empirically that this leads to stable solutions that do not depend much on variations in the used value of γ. This regularization extends the water-level regularization used by Snieder and Şafak (2006) to the system of equations that we solve in the multichannel deconvolution used here. We compute the least-squares solution $\mathbf{x}_{\mathrm{LS}}(\omega)$ for all frequencies. A Fourier transform then gives the time-domain transfer functions $G_{\mathrm{SD}}(t)$, $G_{\mathrm{LT}}(t)$, $G_{\mathrm{LD}}(t)$, and $G_{\mathrm{UT}}(t)$. We repeat the process for the east section to retrieve the structural responses of that section as well.

RETRIEVED TRANSFER FUNCTIONS

The extracted transfer function for the UTs is shown in Figure 4. The transfer function shows two peaks at travel time $t = \pm 0.170$ s. This response can be compared with the transfer function shown in figure 5 of Snieder and Şafak (2006) obtained by deconvolving the motion at the bottom of the

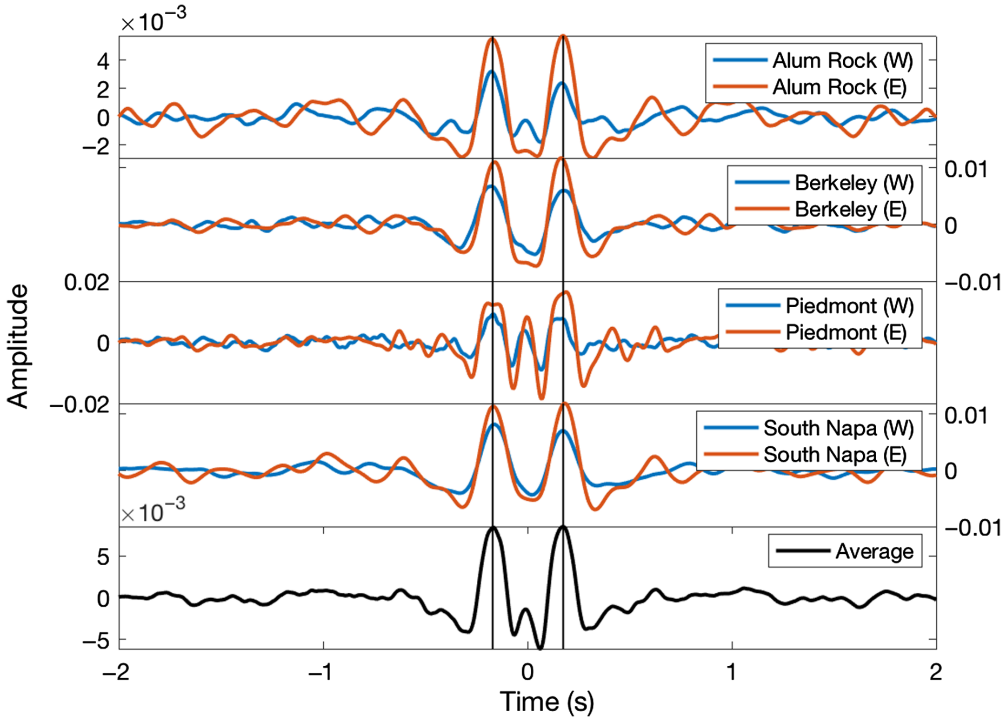

Figure 4. Transfer functions $G_{\mathrm{UT}}(t)$ for the UTs on the west section (W) and the east section (E) retrieved from the four different earthquakes. Bottom panel shows the average of these eight waveforms. The vertical lines show the time of the maximums in the average waveforms at $t = -0.170$ and 0.175 s. The color version of this figure is available only in the electronic edition.

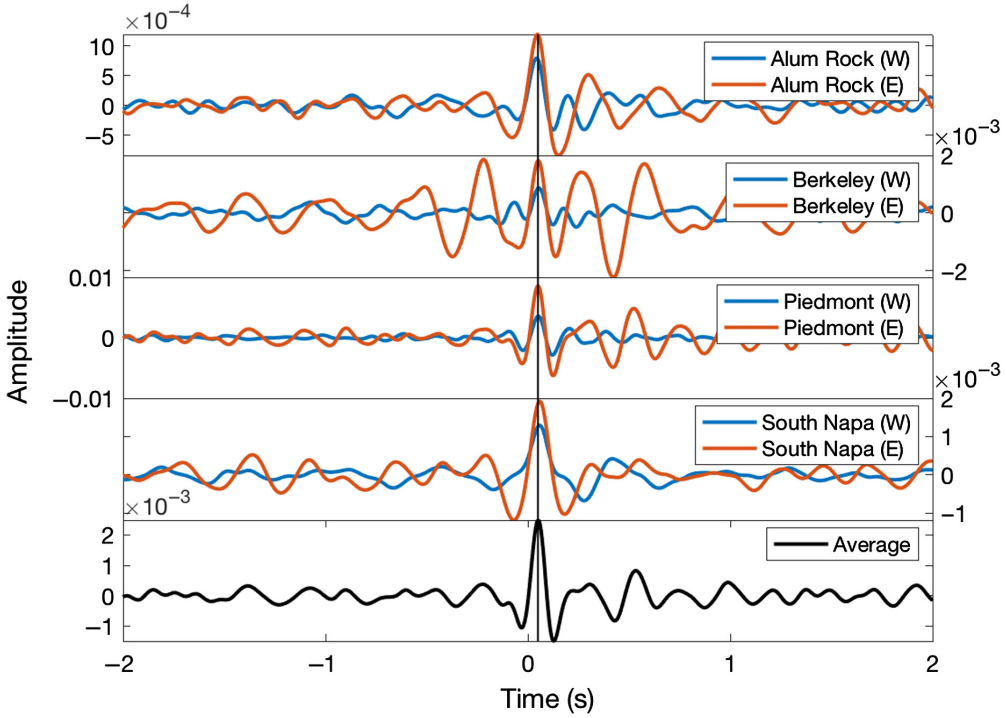

Figure 5. Transfer functions $G_{\mathrm{LT}}(t)$ for the LTs on the west section (W) and the east section (E) retrieved from the four different earthquakes. Bottom panel shows the average of these eight waveforms. The vertical black line shows the time of the maximums in the average waveforms at $t = 0.05$ s. The color version of this figure is available only in the electronic edition.

Millikan Library at Caltech with the motion at the top floor. As in that application, the pulse at negative time corresponds to the wave that propagates from the deck to the top of the tower, whereas the pulse at positive time corresponds to the wave that propagates from the top of the tower to the deck. Given the height of the UTs, the arrival times of these waves correspond to a shear velocity of about 510 m/s.

The transfer functions retrieved from the four different earthquakes, the upper four panels of Figure 4, all show the peaks around $t = \pm 0.170$ s, even though the earthquake data for the four events are independent. Similarly, the peaks in the response functions for the towers in the west section (W) and on the east section (E) are similar. This redundancy provides a consistency check on the retrieval of the transfer function. The average of the eight retrieved transfer functions is shown in the bottom panel of Figure 4; the averaging reduces the noise in the retrieved transfer functions while enhancing the upward and downward propagating waves. The noise level in the deconvolved waveforms in Figure 4 is higher than it is in the deconvolved waveforms of Snieder and Şafak (2006) for the Millikan Library. We attribute this noise to the vibrations that are generated within the bridge, for example, by wind or traffic. Because these internal sources are not accounted for in the theory, this leads to incoherent background noise. The extracted response of the UTs in Figure 4 is slightly larger for the west section than for the east section. This could be caused by a different level of excitation of the two sections of the bridge by the earthquakes that, because of the used regularization, leads to a different strength of the extracted response.

For the Millikan Library, the ratio of the amplitude of the upgoing and downgoing waves could be used to estimate the attenuation in the building (Snieder and Şafak, 2006). In contrast, Figure 4 does not show a clear difference in the amplitude of the upgoing and downgoing waves. Given the used frequencies, the peaks corresponding to the upgoing and downgoing waves are at most two periods apart. For a quality factor $Q = 30$, this would lead to a reduction in amplitude given by $\exp(-\omega t/2Q) = \exp(-\pi t/TQ) \approx 0.8$, in which T denotes the period. Given the noise level of about 20% in the deconvolved waveforms in Figure 4, such a reduction in amplitude cannot be resolved.

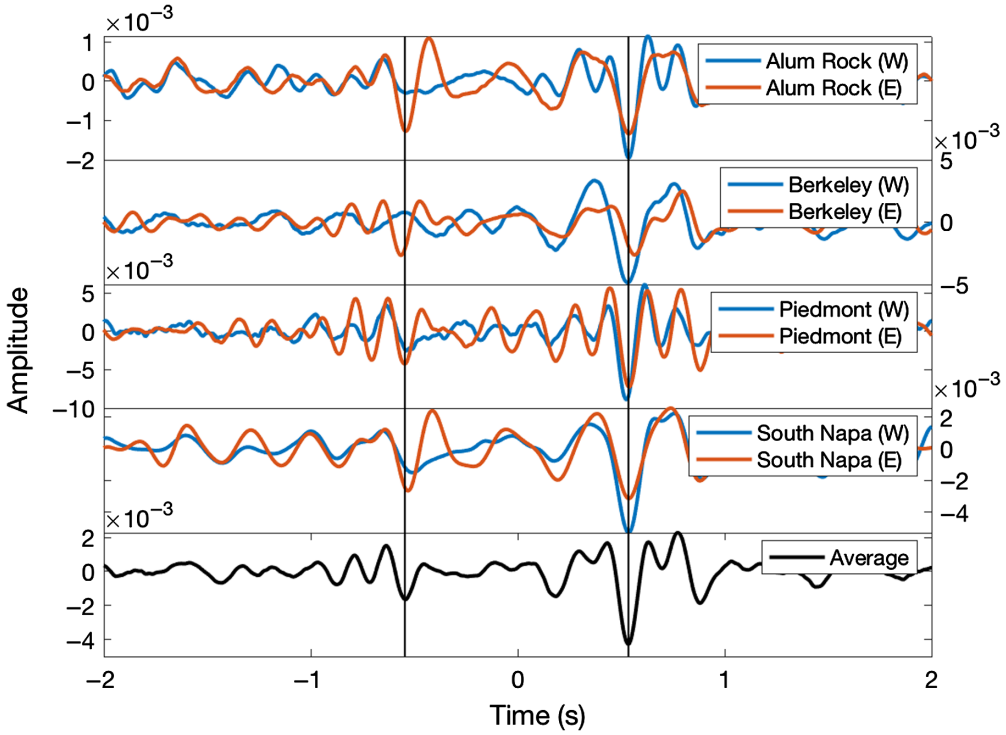

Figure 6. Transfer functions $G_{LD}(t)$ for the long decks on the west section (W) and the east section (E) retrieved from the four different earthquakes. Bottom panel shows the average of these eight waveforms. The vertical lines show the time of the minimums in the average waveforms at $t = -0.545$ and 0.535 s. The color version of this figure is available only in the electronic edition.

We show the extracted transfer function for the LT in Figure 5. The estimated transfer functions for the different earthquakes and the LTs on the east and west side all show a pulse at a time $t = +0.05$ s. For other times, the extracted transfer functions are not coherent. Given the height of the LT, this pulse corresponds to an upward propagating wave that travels with a shear velocity of about 900 m/s (Table 2). This velocity is higher than the shear velocity in the UT, which can be attributed to the stiffer construction of the LT compared to the UT. In contrast to the transfer function for the UT that consists of pulses at positive and negative times (Fig. 4), the transfer function for the LT shows a pulse at positive time only (Fig. 5). The top of the UT is stress free; thus, waves are reflected with a reflection coefficient $R = 1$, and thus a downgoing wave is generated that is comparable to the upgoing wave. In contrast, the top of the LT is at the bridge deck, and an upward propagating wave will partly continue upward in the UT, and it will partly propagate outward along the decks, so that little energy propagates downward.

Figure 6 shows the extracted transfer function of the long deck. As in the case for the UT (Fig. 4), the transfer functions

obtained from different earthquakes and for the east and west sections show two coherent arrivals that are superposed on incoherent fluctuations. The coherent waves arrive at $t = \pm 0.540$ s, which corresponds to a shear velocity of 651 m/s. The incoherent waves in the response for the long deck (Fig. 6) are stronger than for the UT (Fig. 4). This is likely due to the fact that traffic acts as a noise source on the decks. Because internal sources are not included in the system (1), this internal noise produces incoherent arrivals in the extracted transfer functions.

For the east section, the extracted transfer function of the SD is shown in Figure 7. As with the long deck, two coherent waves arrive, now at $t = \pm 0.530$ s. This arrival time corresponds to a shear-wave velocity of 689 m/s (Table 3). This velocity is within 5% of the shear velocity for the long decks, which is not surprising because the decks have a similar structure. For the west section, the extracted response for the SD is so noisy that a coherent wave does not stand out. This may be caused by the noise that is generated by the traffic in this section. Together with the shorter travel times of waves traversing that deck, this noise masks coherent arrivals.

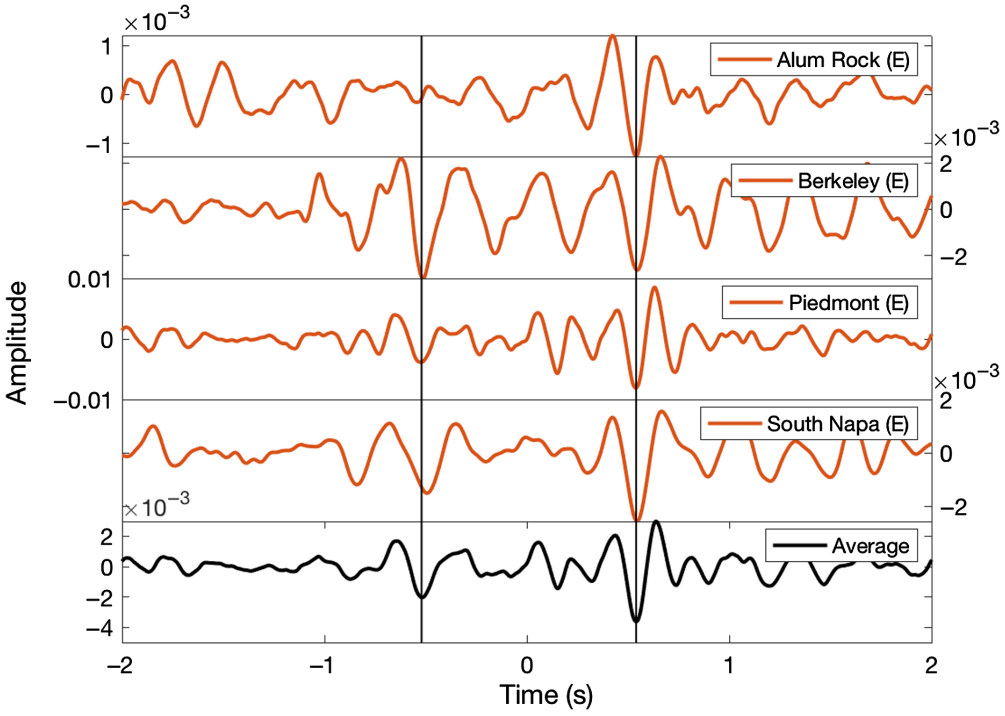

Figure 7. Transfer functions $G_{SD}(t)$ for the SD on the east section retrieved from the four different earthquakes. Bottom panel shows the average of these four waveforms. The vertical lines show the time of the minimums in the average waveforms at $t = -0.520$ and 0.540 s. The color version of this figure is available only in the electronic edition.

DISCUSSION

Although multichannel deconvolution is in general ill-posed, we show that we can use the fact that the Bay Bridge consists of near-identical units (e.g., towers) with the same structure to set up a linear system of equations for the transfer function of these units that is well-posed. The response of the UTs, LTs, and two types of decks extracted from recordings of different earthquakes is similar, and the extracted response for the western section and eastern section of the bridge is similar as well, which provides a consistency check on the estimated transfer functions. The more rigid LT has the largest shear velocity.

The details of the matrix and vectors in equation (1) depend on the mechanical connections within the structure that is studied, as well as on the location and availability of accelerometers. As shown in the Introduction, multichannel deconvolution is, in general, ill-posed. In this study, we used the fact that the Bay Bridge has near-identical towers and decks to make the multichannel deconvolution possible. Whether this is possible for a general instrumented structure depends on the mechanical connections in the structure, the presence of identical elements in the structure, and the locations where the motion is recorded.

We limited the analysis to the motion in the horizontal direction perpendicular to the bridge (the transverse direction). Applying the theory in its current form to the motion in the vertical and inline horizontal directions needs a modification of the theory, and additional sensors. As shown in Figure 2, the cables couple the vertical motion of the deck to the vertical and inline horizontal motion at the top of the towers. This coupling is not taken account in the vectors (equation 4) and the matrix (equation 5). In addition, the motion in the

TABLE 3
Structural Units of the East Section the Transfer Function of which We Estimate

Structural Unit	Name	Segment	Length (m)	Velocity (m/s)
Short deck	SD	aA, dC	379.5, 352.1	689
Long deck	LD	AB, CB	352.1, 352.1	651
Lower tower	LT	bA, cC	47.7, 43.4	910
Upper tower	UT	AD, CE	91.9, 82.7	505

The structural units refer to Figure 1.

vertical direction and in the inline horizontal direction is, in general, coupled at the intersection of the towers and the decks. This coupling also needs to be incorporated into the matrix of expression (5). This means that the theory, in its current form, cannot be applied to the motion in the vertical direction and the inline horizontal direction. The theory can be extended to include the motion in these directions, but additional sensors—for example, at the base of the vertical cables—may be needed to arrive at a system of equations that has stable solutions.

The current deployment of accelerometers does not make it possible to decompose the wavefield into waves propagating in opposite directions. An array of sensors with a spacing less than a wavelength could be used to decompose the wavefield into upgoing and downgoing waves in the towers and into leftgoing and rightgoing waves in the decks. This could be used to decouple the system of equations that one needs to solve. For example, if one knows the leftgoing and rightgoing waves at both ends of a deck, one can set up a system for the transmission of a reflection response of the deck without having to take the coupling of the deck with the tower into account. Arrays of sensors also make it possible to estimate the response of structures under different boundary conditions from those of the real physical structure, and such an array can also be used to estimate intrinsic attenuation. If sensors are available with a spacing significantly less than a wavelength, one can estimate the spatial derivative of the wavefield. Together with the wavefield itself, this derivative can be used to decompose the wavefield into waves that propagate in opposite directions (Robinson, 1999). When this decomposition is known on both sides of structural elements such as a deck, one can determine the properties of that element. Consider for example a deck, as shown in Figure 8, in which pairs of sensors on both ends of a deck are used to decompose the wavefield into waves u_{in} that move into the deck and waves u_{out} that move out of the deck. Let the transmission coefficient for a wave moving to the right be denoted by T and the reflection coefficient for a wave coming in from the right be denoted by R. Then in the frequency domain and in the notation of Figure 8

$$u_{\text{out},R} = T u_{\text{in},L} + R u_{\text{in},R}. \tag{7}$$

This expression presumes there are no sources in the deck, because such source would generate additional outgoing waves. Solving equation (7) for T gives

$$T = \frac{u_{\text{out},R}}{u_{\text{in},L}} - R\frac{u_{\text{in},R}u^*_{\text{in},L}}{|u_{\text{in},L}|^2}, \tag{8}$$

in which the asterisk denotes complex conjugation. $u_{\text{in},R}u^*_{\text{in},L}$ gives the correlation of the waves coming in for the left and from the right. When these waves are uncorrelated, or when the reflection coefficient R vanishes, the last term in expression (8) is equal to zero, and

Figure 8. Decomposition of the wavefield propagating through a deck into incoming and outgoing waves at two locations of the deck. Triangles indicate the location of accelerometers. The color version of this figure is available only in the electronic edition.

$$T = \frac{u_{\text{out},R}}{u_{\text{in},L}}. \tag{9}$$

The transmission operator of the deck thus follows from the deconvolution $u_{\text{out},R}$ with $u_{\text{in},L}$. The phase of the transmission operator gives the wave velocity and its amplitude the attenuation. If the reflection coefficient R is nonzero, one can retrieve the reflection coefficient by solving expression (7) for R to give

$$R = \frac{u_{\text{out},R}}{u_{\text{in},R}} - T\frac{u_{\text{in},L}u^*_{\text{in},R}}{|u_{\text{in},R}|^2}. \tag{10}$$

When the incoming waves on both sides are uncorrelated, $u_{\text{in},L}u^*_{\text{in},R} = 0$, thus

$$R = \frac{u_{\text{out},R}}{u_{\text{in},R}}. \tag{11}$$

This reasoning can be applied to deck elements and towers, which shows that deploying pairs of sensors would obviate the need for the multichannel deconvolution presented in this work.

Using arrays with a sensor spacing much less than a wavelength would provide more accurate estimates of the spatial derivative of the wavefield, and such arrays can also be used to measure the local wave velocity. Decomposing the wavefield into waves propagating in opposite directions also make it possible to estimate the response of structures under different boundary conditions from that of the real physical structure (Snieder *et al.*, 2006) and to estimate intrinsic attenuation (Newton and Snieder, 2012).

Our work shows that the structural response of the Bay Bridge can be estimated from the incoherent excitation of the bridge by earthquakes. This can be used to monitor changes in the response of the bridge by comparing the estimated response functions over time.

DATA AND RESOURCES

We used the data from the Center for Engineering Strong Motion Data (https://cesmd.org, last accessed September 2019).

ACKNOWLEDGMENTS

The authors thank two anonymous reviewers and Editor-in-Chief Thomas Pratt for their critical and constructive comments.

REFERENCES

Bindi, D., B. Petrovic, S. Karapetrou, M. Manakou, T. Boxberger, D. Raptakis, K. D. Pitilakis, and S. Parolai (2015). Seismic response of an 8-story RC-building from ambient vibration analysis, *Bull. Earthq. Eng.* **13,** 2095–2120.

Carder, D. (1936). Observed vibrations of buildings, *Bull. Seismol. Soc. Am.* **26,** 245–277.

Carder, D. (1937). Observed vibrations of bridges, *Bull. Seismol. Soc. Am.* **27,** 267–303.

Clinton, J., S. Case Bredford, T. Heaton, and J. Favela (2006). The observed wander of the natural frequencies in a structure, *Bull. Seismol. Soc. Am.* **96,** 237–257.

Conte, J., R. Astroza, G. Benzoni, G. Feltrin, K. Loh, and B. Moaveni (Editors) (2018). *Experimental Vibration Analysis for Civil Structures*, Springer International Publishing. Cham, Switzerland.

Curtis, A., P. Gerstoft, H. Sato, R. Snieder, and K. Wapenaar (2006). Seismic interferometry—Turning noise into signal, *The Leading Edge* **25,** 1082–1092.

Du, X., G. Li, M. Zhang, H. Li, W. Yang, and W. Wang (2018). Multichannel band-controlled deconvolution based on a data-driven structural regularization, *Geophysics* **83,** R401–R411.

Kirkeby, O., P. A. Nelson, H. Hamada, and F. Orduna-Bustamante (1998). Fast deconvolution of multichannel systems using regularization, *IEEE Trans. Speech Audio Process.* **6,** 189–194.

Kohler, M., P. Davis, and E. Safak (2005). Earthquake and ambient vibration monitoring of the steel-frame UCLA factor building, *Earthq. Spectra* **21,** 1–22.

Kohler, M., T. Heaton, and S. Bradford (2007). Propagating waves in the steel, moment-frame factor building recorded during earthquakes, *Bull. Seismol. Soc Am.* **97,** 1334–1345.

Larose, E., L. Margerin, A. Derode, B. van Tiggelen, M. Campillo, N. Shapiro, A. Paul, L. Stehly, and M. Tanter (2006). Correlation of random wavefields: An interdisciplinary review, *Geophysics* **71,** SI11–SI21.

Luco, J., M. Trifunac, and H. Wong (1987). On the apparent change in dynamic behavior of a 9-story reinforced-concrete building, *Bull. Seismol. Soc. Am.* **77,** 1961–1963.

Lynch, J., Y. Wang, K. J. Loh, J.-H. Yi, and C.-B. Yun (2006). Performance monitoring of the Geumdang Bridge using a dense network of high-resolution wireless sensors, *Smart Mater. Struct.* **15,** 1561.

Nakata, N., and R. Snieder (2014). Monitoring a building using deconvolution interferometry. II: Ambient-vibration analysis, *Bull. Seismol. Soc. Am.* **104,** 204–213.

Nakata, N., R. Snieder, S. Kuroda, S. Ito, T. Aizawa, and T. Kunimi (2013). Monitoring a building using deconvolution interferometry. I: Earthquake-data analysis, *Bull. Seismol. Soc. Am.* **103,** 1662–1678.

Nakata, N., W. Tanaka, and Y. Oda (2015). Damage detection of a building casued by the 2011 Tohoko-Oki earthquake with seismic interferometry, *Bull. Seismol. Soc. Am.* **105,** 2411–2419.

Newton, C., and R. Snieder (2012). Estimating intrinsic attenuation of a building using deconvolution interferometry and time reversal, *Bull. Seismol. Soc. Am.* **102,** 2200–2208.

Prieto, G., J. Lawrence, A. Chung, and M. Kohler (2010). Impulse response of civil structures from ambient noise analysis, *Bull. Seismol. Soc. Am.* **100,** 2322–2328.

Robinson, E. (1999). Seismic inversion and deconvolution, in *Handbook of Geophysical Exploration*, Vol. 4B, Pergamon.

Salvermoser, J., C. Hadzioannou, and S. Stähler (2015). Structural monitoring of a highway bridge using passive noise recordings from street traffic, *J. Acoust. Soc. Am.* **138,** 3864–3872.

Snieder, R., and E. Larose (2013). Extracting Earth's elastic wave response from noise measurements, *Annu. Rev. Earth Planet. Sci.* **41,** 183–206.

Snieder, R., and E. Şafak (2006). Extracting the building response using seismic interferometry; theory and application to the Millikan library in Pasadena, California, *Bull. Seismol. Soc. Am.* **96,** 586–598.

Snieder, R., J. Sheiman, and R. Calvert (2006). Equivalence of the virtual-source method and wave-field deconvolution in seismic interferometry, *Phys. Rev. E* **73,** 066620-1,9, doi: 10.1103/PhysRevE.73.066620.

Sun, H., A. Mordret, G. Prieto, M. Toksöz, and O. Büyüköztürk (2017). Bayesian characterization of buildings using seismic interferometry on ambient vibrations, *Mech. Syst. Signal Process.* **85,** 468–486.

Trifunac, M., S. Ivanović, and M. Todorovska (2003). Wave propagation in a seven-story reinforced concrete building III. Damage detection via changes in wavenumbers, *Soil Dynam. Earthq. Eng.* **23,** 65–75.

Udwadia, F., and M. Trifunac (1974). Time and amplitude dependent response of structures, *Int. J. Earthq. Eng. Struct. Dynam.* **2,** 359–378.

Wenzel, H. (2009). *Health Monitoring of Bridges*, Wiley, Chichester, United Kingdom.

Manuscript received 19 September 2019
Published online 11 February 2020